Causes of the extremely low solar radiation in the 2021 growing season over southeastern Tibetan Plateau and its impact on vegetation growth

Yanyi He[1], Kun Yang[1, 2*], Yanghang Ren[1], Mijun Zou[1], Xu Yuan[1] and Wenjun Tang[2]

[1] Department of Earth System Science, Ministry of Education Key Laboratory for Earth System Modeling, Institute for Global Change Studies, Tsinghua University, 100084 Beijing, China

[2] National Tibetan Plateau Data Center, Key Laboratory of Tibetan Plateau Earth System, Environment and Resources, Institute of Tibetan Plateau Research, Chinese Academy of Sciences, 100101 Beijing, China

[*]**Corresponding Author:** Kun Yang, email: yangk@tsinghua.edu.cn

Bulletin of the American Meteorological Society

Date submitted: May 25, 2022

Date revised: August 22, 2022

Date revised: November 13, 2022

Capsule

The 2021 low solar radiation over southeastern Tibetan Plateau was mainly caused by abnormally strong southerlies and further enhanced by anthropogenic aerosols and GHGs-induced warming, and consequently reduced vegetation growth.

Introduction

The Tibetan Plateau (TP), known as the 'Third Pole' region, is one of the most sensitive places to global climate change (Zhang et al. 2013; Yao et al. 2019), which possesses the highest surface incident solar radiation (SSR) in China but has been dimming in recent decades (Tang et al. 2011; Yang et al. 2012; He and Wang 2020). In the 2021 growing season, i.e., May to September, southeastern Tibetan Plateau (SETP; 29-34°N, 89-102°E; red box in Fig. 1a) registered a widespread and extremely low SSR since 1950 with approximately -18.65 W/m^2 of regional mean anomaly relative to 1950-1979 mean (Fig.1a-1b). Such extreme events are bound to disturb the fragile ecosystem in the SETP (Ren et al. 2021), so it is critical to explore possible causes of this event and its potential impacts on local vegetation growth.

Clouds, aerosols and water vapor have been considered the main contributors to SSR variation (Wild 2009; He et al. 2021b). In the growing season, the South Asian monsoon is particularly prominent for water vapor supply of SETP, thus forming clouds and raining (Lau et al. 2006). Thereby, strong meridional winds from the Bay of Bengal may be responsible for the occurrence of the extreme SSR events like 2021 (Fig. 1c). Besides, human activities may also contribute to an increase in the occurrence probability of such extreme SSR events (Christidis et al. 2016; Takahashi et al. 2019; He et al. 2021a). Emission of anthropogenic greenhouse gases (GHGs) is causing global warming, which is increasing atmospheric water vapor that is favorable to form cloudy days. Anthropogenic aerosols also reduce SSR through absorption and scattering effects (Ramanathan et al. 2001). Based on the aerosol optical depth data from the Moderate Resolution Imaging Spectroradiometer product (MYD08), the aerosol loadings over SETP are greater relative to the past six years (Fig. S1a). Meanwhile, CMIP6 simulations under the anthropogenic aerosol forcing-only scenario (only until 2020) show that SSR driven only by anthropogenic aerosol decreases by -1.30 W/m^2·decade ($p < 0.01$) from 1950 to 2020 (Fig. S1b). Therefore, we also attempted to quantify the roles of anthropogenic forcings, including anthropogenic aerosols and GHGs, in the occurrence probability of the low SSR events like 2021.

The vegetation growth on the TP depends to a large extent on local climate conditions, of

which air temperature, precipitation and solar radiation are the three main climatic factors for vegetation growth (Saleska et al. 2016). Existing researches have suggested that increases in vapor pressure deficit (VPD) rather than changes in precipitation have a greater impact on vegetation productivity (Restaino et al. 2016; Yuan et al. 2019). Solar radiation is the energy source of vegetation photosynthesis, which can directly change the rate of carbon assimilation by plants and in turn leads to significant variations in gross primary productivity (GPP) (Mercado et al. 2009). Thereby, low SSR may interfere with the vegetation growth activities on SETP with the most unique alpine meadow ecosystem in the world. However, the impact of such low SSR events on GPP over SETP has been rarely investigated.

In all, this study aims to explore three questions: 1) How extremely is the low SSR in the 2021 growing season over SETP since 1950? 2) What are the contributions of regional circulation, anthropogenic aerosols, and GHGs-induced warming to the occurrence probability of such SSR events like 2021? 3) What is the impact of the 2021 low SSR event on local GPP?

Data and Methods

Reanalysis products have been widely used in climate studies when observational data are not available, due to their excellent performances in spatiotemporal continuities and inter-annual variability and trends (Zhou et al. 2018). Through developments and applications of the advanced forecast and assimilation systems (IFS Cycle 41r2 and 4D-Var) in the past 10 years, ERA5 has undergone a major upgrade, providing data from 1950 onward with much higher spatial and temporal resolutions than other reanalysis products (Hersbach et al. 2019). ERA5 has been verified to outperform its predecessor ERA-Interim in SSR simulations at monthly, interannual and decadal scales in China (He et al. 2021b). Here, we collected monthly mean SSR observations (only 5 sites available in SETP, Fig. S2a) from the China Meteorological Data Service Center (http://data.cma.cn/en) to confirm that the SSR variation from ERA5 matches well with

observations during 1994-2021and both present the extremely low SSR in the 2021 growing season (Fig. S2b). Because the ground-based observations contain large errors due to the aging and replacement of instruments before 1993 (Tang et al. 2011; Wang 2014; Wang and Wild 2016; He et al. 2018) and significantly lack spatial representation in SETP (Fig. S2a), we finally adopted the monthly SSR of ERA5 reanalysis during 1950-2021 in this study. We chose the earliest possible period, i.e., 1950-1979 with relatively few human activities in SETP (http://www.npc.gov.cn/englishnpc/c2767/200903/979200508a3844d0b21f57b33e6ded94.shtml), as the baseline to calculate their anomalies for better quantifying human influence in the following.

To depict the atmospheric circulation pattern behind the event, the monthly 500 hPa geopotential height (Z500), meridional wind (V500), and zonal wind (U500) and total cloud cover (TCC) from 1950 to 2021 were downloaded from ERA5 (https://www.ecmwf.int/en/forecasts/datasets/reanalysis-datasets/era5). TCC data from MODIS product (MYD08, http://dx.doi.org/10.5067/MODIS/MYD08_M3.006) (Platnick et al. 2015) was used to verify the reliability of the reanalysis TCC (Fig. 1b).

To quantify the impacts of regional circulation, anthropogenic aerosols, and GHGs-induced warming on the extremely low SSR events like 2021, historical simulations with all-forcing (ALL), anthropogenic aerosol forcing-only (AER), GHGs forcing-only (GHG) and natural forcing-only (NAT) from the Coupled Model Intercomparison Project Phase 6 (CMIP6; https://esgf-node.llnl.gov/search/cmip6/) were adopted (Eyring et al. 2016). To ensure an equal weight for different CMIP6 models, the "rlilp1f1" realizations were used in this study. Thirty CMIP6-ALL simulations (Table S1 in the Supplementary Material) were selected based on the comparison of the May-September mean SSR from CMIP6-ALL runs with those from ERA5 via a Kolmogorov-Smirnov test (h = 0 indicates that the test fails to reject the null hypothesis, which is two datasets are from a similar distribution, at the default 5% significance level). Only twelve models are simultaneously available for CMIP6-NAT, CMIP6-AER and CMIP6-GHG simulations (Table S1), and their simulations only last until 2020. The CMIP6-ALL runs only last until 2014, so the ALL

runs were extended to 2021 with the SSP2-4.5 runs that are more consistent with the current climate than other scenarios (O'Neill et al. 2016). The time series and probability density distribution (PDF) of SSR and V500 anomalies from CMIP6-ALL and ERA5 shown in Figure S2 illustrate that their SSR and V500 have comparable probability density distributions, respectively. To be consistent, all data used in this study were converted into 1°×1° grids based on the bilinear interpolation method.

To estimate the occurrence probability (P) and return period (RP = 1/P) of the event, we applied the generalized Pareto distribution (GPD) with a 70% threshold (Schaller et al. 2016) (Zhou et al. 2021) to fit the lower tail (i.e., 30% of data) of the SSR distribution, which can reduce the statistical uncertainty of quantile variances (Brabson and Palutikof 2000). Since the CMIP6-NAT, CMIP6-AER and CMIP6-GHG runs under the SSP2-4.5 scenarios are only available from 3 or 4 models, we selected a window of the last 30 years (1991-2020/2021) instead of a 2021-centered time window (Christidis et al. 2016; Zhou et al. 2021) to ensure enough samples to robustly estimate probability of the event using a 70% GPD fit. We adopted regional mean SSR anomaly in the 2021 growing season over SETP as the threshold (i.e., -18.65 $W \cdot m^{-2}$, as derived from ERA5) of extremely low SSR events for CMIP6-ALL, CMIP6-AER, CMIP6-GHG and CMIP6-NAT runs to explore the causes of this extreme event. Probability ratio is the ratio of event occurrence probabilities between two groups of simulations. It was adopted to assess the contributions of these factors to the event probability. Firstly, we assessed the contribution of south winds by estimating their probability ratios under strong south winds and weak winds based on the 30 CMIP6-ALL runs, i.e., $P_{\mathrm{strongV500}}/P_{\mathrm{weakV500}}$, where $P_{\mathrm{strongV500}}$ is the occurrence probability of SSR being less than the 2021 extreme SSR event under the condition of strong south wind anomalies (V500 ≥ 0.59 m/s, the 2021 regional mean value of ERA5 V500 in dash red box in Fig. 1c) and P_{weakV500} is that under the case of weak wind anomalies between −0.05 and 0.05 m/s. Secondly, we estimated the relative impact of anthropogenic aerosols and GHGs-induced warming on such low SSR events like 2021 by computing probability ratios of CMIP6-AER and CMIP6-

GHG referenced to CMIP6-NAT runs from those 12 models. The 95% confidence intervals (CI) were estimated via bootstrap random resampling with 1000 times.

To explore the impact of the 2021 low SSR event on vegetation growth, we used a state-of-the-art model (i.e., P-model) to simulate changes of gross primary productivities (GPP). Unlike other empirical models, the P-model was developed as a universal model based on the biochemical processes of photosynthesis and the optimality principle (Wang et al. 2017) . The P-model has been widely used (Liu et al. 2019; Peng et al. 2020; Tan et al. 2021; Tan and Wang 2022) and been verified to accurately estimate GPP (Stocker et al. 2020), including the variation of alpine GPP over TP (Ren et al. 2021). More details about the P-model can be seen in Wang et al. (2017). The input data of the P-model include the monthly surface pressure, 2-m air temperature, relative humidity, VPD and SSR from ERA5, fraction of absorbed photosynthetically active radiation (fPAR) from MODIS 8-day products (MOD15A2H), and monthly global CO_2 data from the National Oceanic and Atmospheric Administration (NOAA) during 2015-2021.

Results

During the 1970-2021 growing season, the reginal mean SSR over SETP showed a continuous downward trend (-2.99 $W/m^2 \cdot$decade), and SSR in 2021 registered a new record of the lowest value since 1950 over most areas of SETP (Fig. 1a-b). TCC and V500 anomalies in the 2021 growing season were also abnormally higher than the 1950-1979 mean (Fig. 1b-c), which is most likely due to the strong southerly winds bringing sufficient moisture from the Bay of Bengal to SETP, resulting in cloudy and rainy weather and thus the low SSR. This is also reflected by close and consistent relationships between SSR and V500 across interannual to interdecadal timescales with correlation coefficients from -0.2 to -0.7 ($p < 0.05$) (Fig. 1b). Based on the 70% GPD fit of the observed SSR anomalies, we found that the extremely low SSR event for the 2021 growing season in SETP is a 1-in-284-year event (95% CI: 82-∞) (Fig. 1d). The large uncertainty in this

return period is mainly ascribed to the small sample size or being too extreme in the 2021 event which has not been found in previous events.

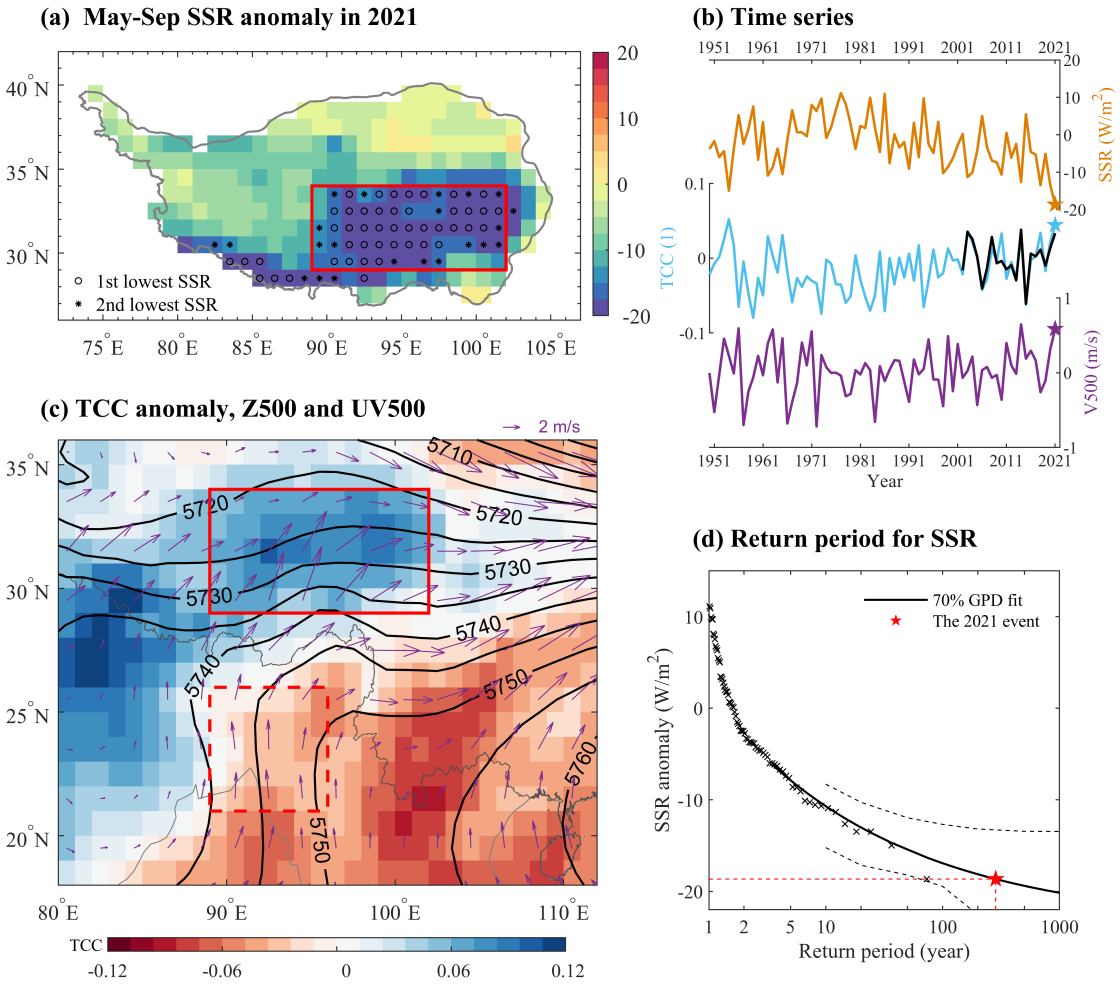

Figure 1. (a) Spatial distribution of the surface incident solar radiation (SSR; W/m^2) anomalies in May-September 2021. "○" and "*" represent the 2021 SSR values are the first and second lowest SSR records since 1950, respectively. (b) Time series of May-September mean SSR (in W/m^2; orange curve), total cloud cover (TCC; in Unit 1; blue for ERA5 and black for MODIS) anomalies averaged in SETP (red box in Fig. 1a) from 1950 to 2021. The purple curve denotes the 500 hPa meridional wind anomalies (V500; m/s) averaged in red dashed box in Fig. 1c. The 2021 values are shown as pentagram. (c) Spatial distribution of TCC anomalies (shading; in Unit 1), the 500 hPa geopotential height (Z500; in meters; contours) and wind vector (UV500; in m/s; vectors) in

May-September 2021. (d) Generalized Pareto distribution (GPD) fit of the SSR anomalies. The 95% confidence intervals are shown as dash curves and the SSR value for May-September 2021 is shown as red pentagram.

To quantify the contribution of anomalous south winds in such SSR events like 2021 over SETP, we compared the return periods of such low SSR events like 2021 between two conditions with strong south wind anomalies (V500 $\geq$ 0.59 m/s; purple in Fig. 2a) and weak wind anomalies (-0.05 m/s $\leq$ V500 $\leq$ 0.05 m/s; light purple in Fig. 2a), and found that the best estimates of the occurrence probability of such SSR events below the 2021 threshold (i.e., -18.65 $W \cdot m^{-2}$) are 6.17% (95% CI: 1.81%-9.95%) and 0.67% (95% CI: 0.001%-1.52%), respectively. This indicates that anomalous south winds could substantially increase the chance of such events to be a factor of 9.25 (95% CI: 6.56-19.02) (Fig. 2b), suggesting that south winds play a key role in causing the low SSR over SETP through propagating large amounts of atmospheric moisture to SETP from the Bay of Bengal. It's worth noting that anthropogenic forcing did not significantly change the likelihood of such anomalous south winds like 2021 (Fig. S3).

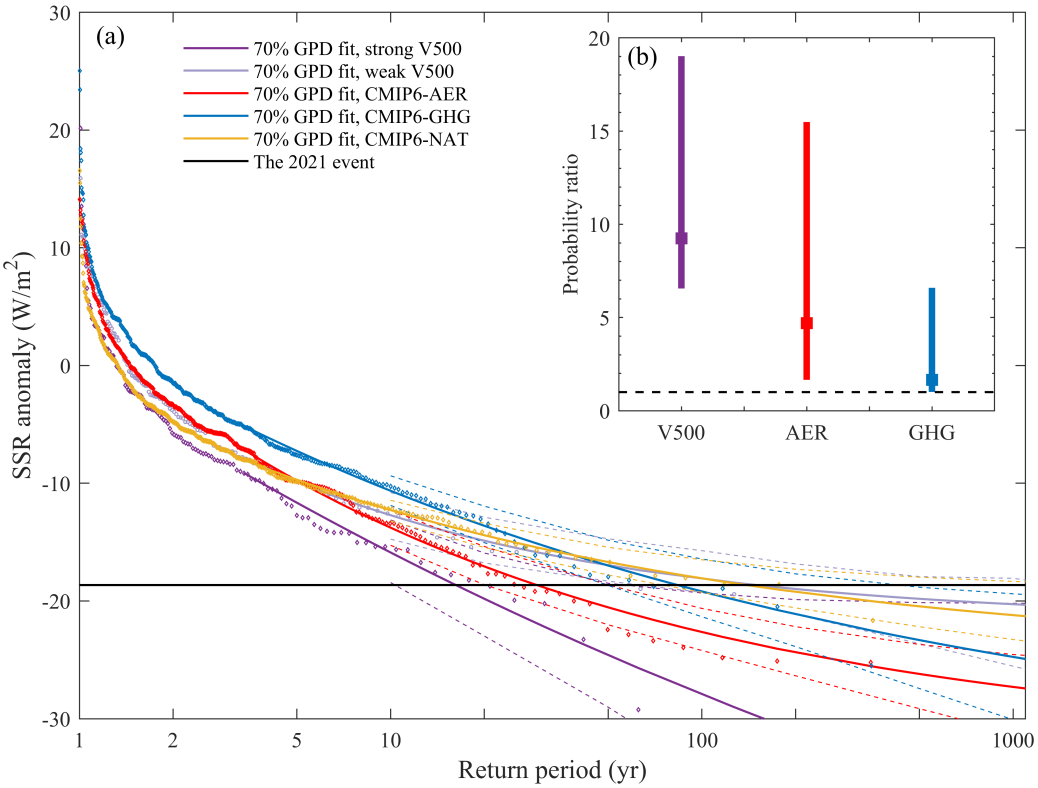

178

179 **Figure 2.** (a) Return period for the regional mean surface incident solar radiation anomalies (SSR;
180 W/m^2; dots) from CMIP6 historical climate simulations under different scenarios, including
181 anthropogenic aerosol forcing-only runs (AER; red), GHGs forcing-only runs (CMIP6-GHG; blue)
182 and natural forcing-only runs (NAT; yellow) and their GPD fits are shown as solid curves with the
183 95% confidence intervals in dash curves. The deep purple and light purple curves represent the 70%
184 GPD fits under two conditions with strong south wind anomalies ($V500 \geq 0.59$ m/s, the 2021 value)
185 and weak wind anomalies (-0.05 m/s $\leq$ V500 $\leq$ 0.05 m/s) in the CMIP6 all-forcing climate
186 simulations, respectively. The black horizonal line is the observed SSR averaged in May-
187 September 2021. (b) Probability ratios of such extreme SSR events like 2021 due to the occurrence
188 of strong south winds (V500; purple), anthropogenic aerosols (AER; red) and GHGs-induced
189 warming (GHG; blue). The bottom and top edges of the bar indicate the 95% confidence intervals.
190 The black dashed line represents the probability ratio equal to 1.

191

192 Comparisons of the probabilities of such SSR events between CMIP6-AER/CMIP6 GHG and
193 CMIP6-NAT runs can infer the impacts of anthropogenic aerosols and global warming on the 2021

194 low SSR event. Based on the GPD fit, such SSR events in the CMIP6-AER and CMIP6-GHG runs
195 are more likely to occur than in CMIP6 NAT runs (Fig. 2a). The best estimates of the occurrence
196 probabilities of the SSR anomalies to be less than the 2021 threshold are 3.40% (95% CI: 2.00%-
197 4.97%), 1.20% (95% CI: 0.24%-2.05%) and 0.72% (95% CI: 0.04%-1.36%) for CMIP6-AER,
198 CMIP6-GHG and CMIP6-NAT runs, respectively. The probability ratios of such SSR events like
199 2021 due to anthropogenic aerosol and global warming are 4.70 (95% CI: 1.66-15.49) and 1.66
200 (95% CI: 1.01-6.59), respectively (Fig. 2b). This indicates that anthropogenic aerosols and the
201 increased atmospheric water vapor due to GHG-induced warming could further make such low
202 SSR events occur more likely in SETP.

203 As the main energy source of vegetation photosynthesis, extreme SSR conditions are bound
204 to change local GPP. Compared to the average of the recent six years (2015-2020), GPP in 2021
205 growing season apparently decreased in the eastern SETP but increased in the western SETP (Fig.
206 3a). SSR in the 2021 growing season presented negative values in the whole SETP (Fig. 3c), which
207 significantly resulted in an extensively decreased GPP (Fig. 3b). The difference of GPP between
208 Fig. 3a and 3b mainly resulted from other influencing factors including air temperature, VPD and
209 fPAR (Fig. 3d-f). For dry western SETP, vegetation growth activities are more limited by water
210 availability (Yao et al. 2019), so the reduction of VPD (Fig. 3e) promotes stomatal opening to
211 enhance carbon uptake and water use efficiency of plants (Konings et al. 2017; Yuan et al. 2019).
212 Along with the increase of fPAR (Fig. 3f), GPP increased in these western SETP (Fig. 3a). For
213 humid eastern SETP, SSR could be a stronger stress factor for vegetation photosynthesis (Ren et
214 al. 2021), thereby the extremely low SSR plays a major role in the GPP reduction in the 2021
215 growing season over eastern SETP (Fig. 3a and 3c). Note that air temperature, SSR, and VPD not
216 only directly influence the photosynthesis rate, but also indirectly cause changes in GPP through
217 altering fPAR.

218

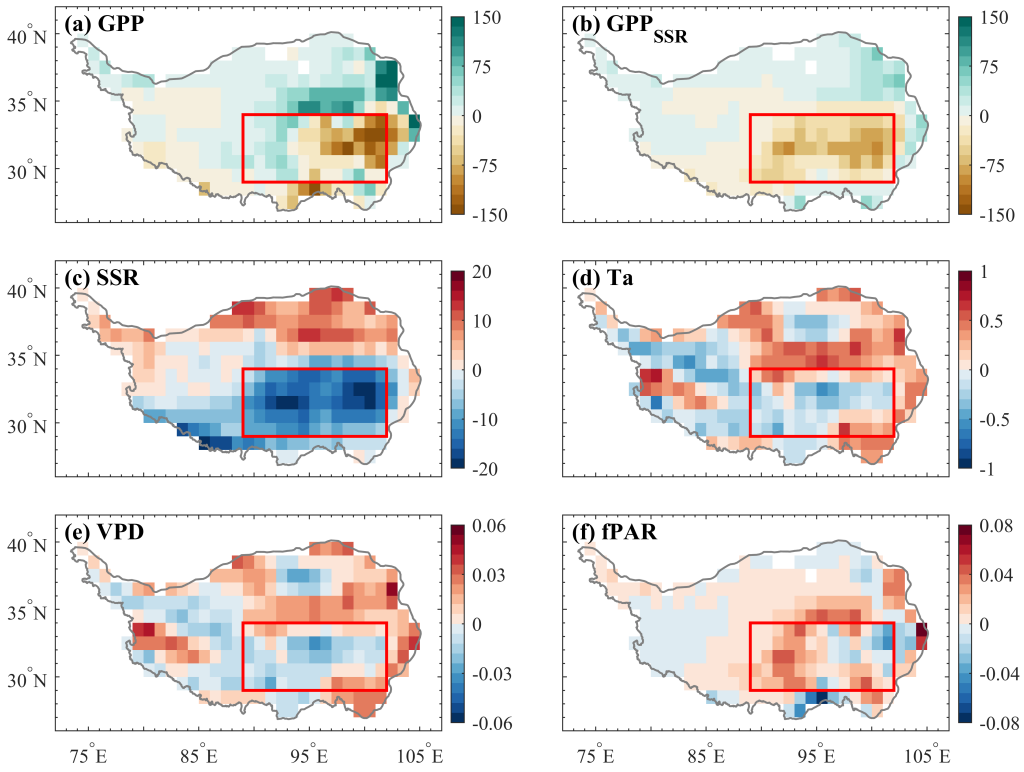

219

220 **Figure 3.** (a) Spatial distribution of the cumulative gross primary productivity (GPP; g C/m^2)
221 changes in the 2021 growing season relative to the 2015-2020 mean. (b) As in (a), but for GPP
222 changes only influenced by surface incident solar radiation (SSR). (c-f) As in (a), but for the
223 anomalies of SSR (W/m^2), 2-m air temperature (Ta; ℃), vapor pressure deficit (VPD; kPa) and
224 fraction of absorbed photosynthetically active radiation (fPAR), respectively.

225

226 **Conclusions**

227 The SSR in the 2021 growing season registered a new low record in southeastern Tibetan
228 Plateau with -18.65 W/m^2 relative to the 1950-1979 mean. Through the analyses using
229 observations, reanalysis and CMIP6 model simulations, the extremely low SSR event in 2021 is
230 mainly attributed to more clouds and abundant atmospheric moisture caused by anomalous
231 southerlies from the Bay of Bengal. The existence of abnormal south winds could increase the
232 probability ratio of such low SSR events like 2021 to be 9.25 (95% CI: 6.56-19.02). Anthropogenic

aerosols and GHGs-induced warming might increase the probability of such SSR events to be a factor of 4.70 (95% CI: 1.66-15.49) and 1.66 (95% CI: 1.01-6.59), respectively. As a result, the extremely low SSR event could significantly reduce local GPP in the 2021 growing season over SETP, especially in the humid eastern SETP where SSR has a stronger impact on vegetation photosynthesis.

The uncertainties could exist in our attribution analysis based on climate simulations. Specifically, data accuracy of external forcings including anthropogenic aerosols and greenhouse gases used in climate models and model skills of simulating related physical processes could introduce attribution uncertainties to some extent. Moreover, although SETP is sparsely populated, the use of the 1950-1979 baseline period to calculate the anomalies might still underestimate the contribution of anthropogenic forcing in the probability of such events, since there's still some anthropogenic effect during this baseline period. Finally, due to the unavailability of CMIP6 simulations with individual forcing after 2021, the use of a window of the recent 30 years instead of a 2021-centered time window probably underestimates the roles of these external forcings slightly.

Acknowledgements

This study was supported by the National Natural Science Foundation of China (No. 42205171), the China Postdoctoral Science Foundation (No. 2021M701839), the Shuimu Tsinghua Scholar Program, and the National Key R&D Program of China (No. 2018YFA0605400). CMIP6 model data were obtained at https://esgf-node.llnl.gov/projects/cmip6/. The ERA5 data were obtained at https://www.ecmwf.int/en/forecasts/datasets/reanalysis-datasets/era5. MODIS data were obtained at https://modis.gsfc.nasa.gov/data/dataprod/mod08.php.

References

Brabson, B. B., and J. P. J. J. o. A. M. Palutikof, 2000: Tests of the Generalized Pareto Distribution for

Predicting Extreme Wind Speeds. *Journal of Applied Meteorology*, **39,** 1627-1641.

Christidis, N., M. McCarthy, A. Ciavarella, and P. A. Stott, 2016: Human contribution to the record sunshine of winter 2014/15 in the United Kingdom. *Bull. Am. Meteorol. Soc.*, **97,** S47-S50.

Eyring, V., S. Bony, G. A. Meehl, C. A. Senior, B. Stevens, R. J. Stouffer, and K. E. Taylor, 2016: Overview of the Coupled Model Intercomparison Project Phase 6 (CMIP6) experimental design and organization. *Geosci. Model Dev.*, **9,** 1937-1958.

He, Y., and K. Wang, 2020: Variability in direct and diffuse solar radiation across China from 1958 to 2017. *Geophys. Res. Lett.*, **47,** e2019GL084570.

He, Y., K. Wang, and D. Qi, 2021a: Roles of anthropogenic forcing and natural variability in the record-breaking low sunshine event in January–February 2019 over the Middle-Lower Yangtze Plain. *Bull. Am. Meteorol. Soc.*, **102,** S75-S81.

He, Y., K. Wang, and F. Feng, 2021b: Improvement of ERA5 over ERA-Interim in simulating surface incident solar radiation throughout China. *J. Clim.*, **34,** 3853–3867.

He, Y., K. C. Wang, C. L. Zhou, and M. Wild, 2018: A revisit of global dimming and brightening based on the sunshine duration. *Geophys. Res. Lett.*, **45,** 4281-4289.

Hersbach, H., and Coauthors, 2019: Global reanalysis: goodbye ERA-Interim, hello ERA5. *ECMWF Newsletter*, **159,** 17-24.

Konings, A. G., A. P. Williams, and P. Gentine, 2017: Sensitivity of grassland productivity to aridity controlled by stomatal and xylem regulation. *Nat. Geosci.*, **10,** 284-288.

Lau, K. M., M. K. Kim, and K. M. Kim, 2006: Asian summer monsoon anomalies induced by aerosol direct forcing: the role of the Tibetan Plateau. *Clim. Dyn.*, **26,** 855-864.

Liu, Y. W., and Coauthors, 2019: Field-experiment constraints on the enhancement of the terrestrial carbon sink by CO2 fertilization. *Nat. Geosci.*, **12,** 809-814.

Mercado, L. M., N. Bellouin, S. Sitch, O. Boucher, C. Huntingford, M. Wild, and P. M. Cox, 2009: Impact of changes in diffuse radiation on the global land carbon sink. *Nature*, **458,** 1014-1017.

O'Neill, B. C., and Coauthors, 2016: The Scenario Model Intercomparison Project (ScenarioMIP) for CMIP6. *Geosci. Model. Dev.*, **9,** 3461-3482.

Peng, Y. K., K. J. Bloomfield, and I. C. Prentice, 2020: A theory of plant function helps to explain leaf-trait and productivity responses to elevation. *New Phytol.*, **226,** 1274-1284.

Platnick, S., K. M. P. Hubanks, and M. D. King, 2015: MODIS Atmosphere L3 Monthly Product (08_L3). NASA MODIS Adaptive Processing System, Goddard Space Flight Center, USA: http://dx.doi.org/10.5067/MODIS/MYD08_M3.006

Ramanathan, V., P. J. Crutzen, J. T. Kiehl, and D. Rosenfeld, 2001: Atmosphere-aerosols, climate, and the hydrological cycle. *Science*, **294,** 2119-2124.

Ren, Y., K. Yang, H. Wang, L. Zhao, Y. Chen, X. Zhou, and Z. La, 2021: The South Asia Monsoon Break Promotes Grass Growth on the Tibetan Plateau. *J. Geophys. Res. Biogeosci.*, **126,** e2020JG005951.

Restaino, C. M., D. L. Peterson, and J. Littell, 2016: Increased water deficit decreases Douglas fir growth throughout western US forests. *P. Natl. Acad. Sci. USA.*, **113,** 9557-9562.

Saleska, S. R., J. Wu, K. Y. Guan, A. C. Araujo, A. Huete, A. D. Nobre, and N. Restrepo-Coupe, 2016: Dry-season greening of Amazon forests. *Nature*, **531,** E4-E5.

Schaller, N., and Coauthors, 2016: Human influence on climate in the 2014 southern England winter floods and their impacts. *Nat. Clim. Change*, **6,** 627-634.

Stocker, B. D., and Coauthors, 2020: P-model v1.0: an optimality-based light use efficiency model for simulating ecosystem gross primary production. *Geosci. Model Dev.*, **13,** 1545-1581.

Takahashi, C., and Coauthors, 2019: The effects of natural variability and climate change on the record low sunshine over Japan during August 2017. *Bull. Am. Meteorol. Soc.*, **100,** S67-S71.

Tan, S., and H. Wang, 2022: Towards a universal model for estimating Gross Primary Productivity and evapotranspiration coupling based on First-Principles Theory. *Acta Ecologica Sinica*, **42,** 1487-1499.

Tan, S., H. Wang, I. C. Prentice, and K. Yang, 2021: Land-surface evapotranspiration derived from a first-principles primary production model. *Environ. Res. Lett.*, **16**.

Tang, W. J., K. Yang, J. Qin, C. C. K. Cheng, and J. He, 2011: Solar radiation trend across China in recent decades: a revisit with quality-controlled data. *Atmos. Chem. Phys.*, **11,** 393-406.

Wang, H., and Coauthors, 2017: Towards a universal model for carbon dioxide uptake by plants. *Nature Plants*, **3,** 734-741.

Wang, K., 2014: Measurement biases explain discrepancies between the observed and simulated decadal variability of surface incident solar radiation. *Sci. Rep.*, **4,** 6144.

Wang, Y., and M. Wild, 2016: A new look at solar dimming and brightening in China. *Geophys. Res. Lett.*, **43,** 11,777-711,785.

Wild, M., 2009: Global dimming and brightening: A review. *J. Geophys. Res. Atom.*, **114,** D00D16.

Yang, K., B. H. Ding, J. Qin, W. J. Tang, N. Lu, and C. G. Lin, 2012: Can aerosol loading explain the solar dimming over the Tibetan Plateau? *Geophys. Res. Lett.*, **39**.

Yao, T. D., and Coauthors, 2019: Recent Third Pole's Rapid Warming Accompanies Cryospheric Melt and Water Cycle Intensification and Interactions between Monsoon and Environment: Multidisciplinary Approach with Observations, Modeling, and Analysis. *Bull. Am. Meteorol. Soc.*, **100,** 423-444.

Yuan, W., and Coauthors, 2019: Increased atmospheric vapor pressure deficit reduces global vegetation growth. *Sci. Adv.*, **5**.

Zhang, G. L., Y. J. Zhang, J. W. Dong, and X. M. Xiao, 2013: Green-up dates in the Tibetan Plateau have

continuously advanced from 1982 to 2011. *P. Natl. Acad. Sci. USA.*, **110,** 4309-4314.

Zhou, C., Y. He, and K. Wang, 2018: On the suitability of current atmospheric reanalyses for regional warming studies over China. *Atmos. Chem. Phys.*, **18,** 8113-8136.